Original Article

Institution of MECHANICAL ENGINEERS
Journal of ENGINEERING MANUFACTURE

Proc IMechE Part B:
J Engineering Manufacture
1–16

DOI: 10.1177/0954405415598945
pib.sagepub.com
SAGE

Contact-state modelling in force-controlled robotic peg-in-hole assembly processes of flexible objects using optimised Gaussian mixtures

Ibrahim F Jasim, Peter W Plapper and Holger Voos

Abstract

This article proposes the distribution similarity measure–based Gaussian mixtures model for the contact-state (CS) modelling in force-guided robotic assembly processes of flexible rubber parts. The wrench (Cartesian force and torque) signals of the manipulated object are captured for different states of the given assembly process. The distribution similarity measure–based Gaussian mixtures model CS modelling scheme is employed in modelling the captured wrench signals for different CSs. The proposed distribution similarity measure–based Gaussian mixtures model CS modelling scheme uses the Gaussian mixtures model in modelling the captured signals. The parameters of the Gaussian mixtures models are computed using expectation maximisation. The optimal number of Gaussian mixtures model components for each CS model is determined by considering the classification success rate as an index for the similarity measure between the distribution of the captured signals and the developed models. The optimal number of Gaussian mixtures model components corresponds to the highest classification success rate; hence, object elasticity variation would be accommodated by properly choosing the optimal number of Gaussian mixtures model components. The performance of the proposed distribution similarity measure–based Gaussian mixtures model CS modelling strategy is evaluated by a test stand composed of a KUKA lightweight robot doing peg-in-hole assembly processes for flexible rubber objects. Two rubber objects with different elasticity are considered for two experiments; in the first experiment, an elastic peg of 30 Shore A hardness is considered and that of the second experiment has hardness of 6 Shore A which is even softer than the one used in experiment 1. Employing the proposed distribution similarity measure–based Gaussian mixtures model CS modelling strategy excellent classification success rate was obtained for both experiments. However, more Gaussian mixtures model components are required for the softer one that gives a strong impression of the non-stationarity behaviour increment for softer materials. Comparison is performed with the available CS modelling schemes and the distribution similarity measure–based Gaussian mixtures model is shown to provide the best classification success rate performance with a reduced computational time.

Keywords

Expectation maximisation, distribution similarity measure, flexible objects assembly, force-controlled robots, Gaussian mixture, peg-in-hole

Date received: 11 October 2014; accepted: 13 July 2015

Introduction

Robotic assembly attracted the interest of both academia and industry, due to its vital role in automating the production for many processes. Excellent robotic assembly strategies were reported in the literature that use different kinds of vision and laser sensors in order to have a precise location of the mated parts (see Biao et al.,[1] Muelaner et al.,[2] Jayaram and Joshi,[3] and the references therein). However, force-controlled robots appear to be one of the efficient systems in assembly, since it handles processes when the vision systems become less accurate. Parts occlusion, unclean environment in the industry, and variable illuminations

Faculty of Science, Technology and Communication, University of Luxembourg, Campus Kirchberg, Luxembourg

Corresponding author:
Ibrahim F Jasim, Faculty of Science, Technology and Communication, University of Luxembourg, Campus Kirchberg, L-1359 Luxembourg.
Email: ibrahim.jasim@uni.lu

constitute the main reasons of vision systems performance degradation, which is motivating the use of the force-controlled robots. In order to accommodate position uncertainties, passive compliance wrists were built for peg-in-hole assembly processes that would facilitate the mating process with position uncertainties.[4,5] In many assembly processes, using passive compliance wrist alone might not stand a chance that necessitate adding a kind of perception to the force-guided robotic assembly. An abstract knowledge or perception of the environment can be added to the robot using the sensed wrench (Cartesian force and torque), pose (Cartesian position and orientation), and/or twist (linear and angular velocity) signals of the manipulated object. The addition of such abstract knowledge is realised by contact-state (CS) modelling of the robot with respect to its surrounding environment. However, CS modelling in force-controlled robots is rooted back to the 1980s.

Desai and Volz[6] proposed a significant milestone in transferring skills to the compliant motion robots by introducing the notion of the contact formation (CF). For instance, if one has a polyhedral manipulated object interacting with a certain environment, then one can describe the contact of the object vertex to the face of the environment and call it as a vertex–face (*v–f*) contact. Likewise to the edge–face (*e–f*), face–face (*f–f*), edge face–2faces (*ef–2f*), 2faces–2faces (*2f–2f*), 3faces–3faces (*3f–3f*), and other possible contacts. Each one of these contact phases is called as CF, and a force-controlled robotic assembly task can be composed by these set of CFs. Hirai and Iwata[7] proposed a CS modelling scheme for such robotic systems using the geometric model of the manipulated object along with the sensed force signals. Petri net was successfully employed in modelling and planning force-controlled robotic assembly tasks, and promising results were obtained.[8,9] Uncertainties were accommodated for such modelling tasks through developing a CS modelling system that relies on incorporating the sensed forces, the sensed error signals, and the contact compliance.[10] The concept of discrete event systems was adroitly used in producing efficient CS models.[11,12]

Hovland and McCarragher,[13] Skubic and Volz,[14] Skubic et al.,[15] and Iwata and Sugano[16] used neural networks in building CS modelling systems of compliant motion robots. Relying on the task sequence, local depart space (LDS) was successfully utilised in recognising the CSs with accommodating possible uncertainties.[17] Skubic and Volz,[14] Skubic et al.,[15] Xiao and Liu,[18] Everett et al.,[19] Skubic and Volz,[20] and Son[21] employed fuzzy classifiers in recognising different CSs for different objects without needing the geometrical features of the manipulated object. Modelling of different contacts in robotic peg-in-hole assembly process was successfully performed in the framework of finding analytical solutions of the contact forces for different situations between the manipulated object and the environment.[22,23] Cortesão et al.[24] used a neural network and Kalman filter in building a signal diffusion system that captures human skills in compliant motion robots. Hidden Markov models (HMM) were successfully employed in developing models for compliant motion robots, and hence, opening the door to the probabilistic modelling approaches.[25–27] HMM CS modelling scheme proved to be efficient and only the previous state (CS) is required to be known when recognising a certain CS.

Gadeyne et al.[28] and Lefebvre et al.[29] were successful in linking the CS modelling to the geometrical parameters estimation, and efficient models were obtained for each CS. The approaches by Gadeyne et al.[28] and Lefebvre et al.[29] were further improved using the particle filters in identifying the CS for compliant motion robots.[30] Despite of their good performance, the approaches proposed by Gadeyne et al.,[28] Lefebvre et al.,[29] and Meeussen et al.[30] require the precise knowledge of the task sequence that would constitute a drawback when using those schemes for variable task sequence which could be the case in many applications. Thomas et al.[31] developed force/torque mapping for each model using computer-aided design (CAD) data with particle filters, and enhanced CS modelling was obtained. Katsura et al.[32] proposed a disturbance observer–based approach in monitoring the contacts of the robot without the need for using force sensors. Autoregressive exogenous (ARX) modelling was successfully employed in adding the recognition skills to the robotic peg-in-hole assembly tasks and promising results were obtained.[33]

Cabras et al.[34] were capable of using the stochastic gradient boosting (SGB) classifier in modelling different CSs without the need for knowing the task sequence or task graph. Hertkorn et al.[35] used only the force and torque signals in recognising different CSs for compliant motion robot systems by computing the wrench space based on the CS graph that describes the sequence of different CSs in a certain task. Then, a similarity index is augmented showing the amount of overlap between wrenches that belong to different CSs. Finally, a particle filter is employed in computing the likeness that a certain wrench vector belongs to a CS. The results shown in Hertkorn et al.[35] are excellent for the computation time wise; however, the sequence of the CSs is still needed to be known. Support vector machine (SVM) was successfully employed in generating the fuzzy inference mechanism (FIM) for classifying the contacts in a force-controlled robotic peg-in-hole assembly process.[36]

A common feature to all of the approaches above is the lack of considering objects flexibility that would result in a more challenging modelling situation. Both vision and force sensors were employed in the CS transition detection for deformable manipulated parts (see Abegg et al.[37] and the references therein). Even though good results were reported by Abegg et al.[37] for a hose assembly process, the strategy does not depend purely on the force signals and using the vision system might

not stand a chance for unclean industrial environments, occluded parts assembly, and assembly processes with a time-varying illumination as mentioned above. Variation in the assembly sequence would also lead to the incapability of applying the scheme reported by Abegg et al.[39] for the assembly CS recognition.

Jasim and Plapper[38] were successful in using fuzzy clustering technique for building efficient fuzzy models and the need for the assembly sequence is relaxed. The fuzzy clusters are tuned by the gravitational search algorithm (GSA), and excellent mapping capability was obtained for each model. Relying on the sensed pose and wrench signals, expectation maximisation–based Gaussian mixtures model (EM-GMM) was proposed for the assembly of multiple rigid parts, and excellent performance was reported.[39] Based on the EM-GMM CS modelling scheme proposed by Jasim and Plapper,[39] only wrench signals were employed with the EM-GMM CS modelling scheme for the hole position identification problem and large position uncertainties were accommodated.[40] Despite the excellent modelling and search performance reported by Jasim and colleagues,[39,40] the number of GMM components was considered to be arbitrarily 3 that might not reflect the optimal choice for such a modelling process in which all manipulated objects are rigid parts. Even though efficient CS modelling was reported by Jasim and colleagues,[38–40] only rigid manipulated objects were considered and accommodating the object flexibility is not yet addressed.

Object flexibility leads to a more challenging CS modelling situation since the sensed signals would be significantly impacted with the object elasticity resulting in higher non-stationarity in the signals distribution and fixing the number of GMM components (as proposed in Jasim and colleagues[39,40]) might not be enough for modelling the captured signals distribution. Inspired by the similarity measure between the developed models and the distribution of the captured signals, this article proposes a distribution similarity measure–based Gaussian mixtures model (DSM-GMM) CS modelling scheme for peg-in-hole assembly tasks of flexible rubber materials. Only the wrench signals of the manipulated object are utilised in developing the models of the DSM-GMM so that more robustness against position uncertainty is achieved. Different numbers of GMM components are studied and the classification success rate (CSR) is considered as an index for measuring the similarity between the developed models and the distribution of the captured signals. For each number of GMM components, the expectation maximisation (EM) algorithm is used in computing the GMM parameters. The number of GMM components resulting with the highest CSR is considered as the optimal number of components and the obtained model is said to be an optimal GMM model. Hence, the DSM-GMM is an optimised modelling scheme compared to the EM-GMM proposed in Jasim and colleagues[39,40] and elasticity variation from an object to another can be accommodated through finding the number of GMM components that optimally model the given input data. As a summary, the contributions of this article are summarised as follows:

1. Developing CS modelling scheme for elastic rubber objects;
2. Finding the number of GMM components that optimally model the captured data.

Experimental validation is carried out on a KUKA lightweight robot (LWR) doing two peg-in-hole assembly experiments of elastic rubber objects. In the first experiment, the robotic peg-in-hole assembly process for an elastic object is considered. The object is made from a rubber silicone material with hardness of 30 Shore A. For the second experiment, a softer rubber silicon material with hardness of 6 Shore A is considered for the relevant robotic peg-in-hole assembly task. For both experiments, DSM-GMM is used in modelling different phases and excellent modelling performance is demonstrated. The available CS modelling schemes are also implemented in order to have a clear comparison study with the proposed DSM-GMM CS modelling scheme. Conventional fuzzy classifier (CFC),[20] SGB classifier,[34] gravitational search-fuzzy clustering algorithm (GS-FCA) classifier,[38] and support vector machine–based fuzzy inference mechanism (SVM-FIM)[36] are implemented for the considered experiments, and the superiority of the proposed DSM-GMM CS modelling scheme is shown.

The rest of this article is organised as follows: section 'Problem description' describes the CS modelling problem in force-controlled peg-in-hole assembly processes with flexible rubber object. Section 'DSM-GMM' explains the proposed DSM-GMM CS modelling scheme and the experimental validation is detailed in section 'Experimental validation'. Discussions of the results obtained from the experimental validation are explained in section 'Discussion,' and 'Conclusion' summarises the concluding remarks along with recommendations for future works.

Problem description

Consider the robot system shown in Figure 1 which is composed of a KUKA LWR doing a peg-in-hole assembly process of a flexible rubber object. If one drives the robot to assemble the peg into the hole, then different possible phases could be brought about during the task execution. In order to model the CS for each phase, the overall motion is segmented according to the corresponding phases. For each segment, the wrench signals of the manipulated object are collected and the models, realising the desired input–output mapping, are developed. Suppose that the Cartesian force signals of the manipulated object are

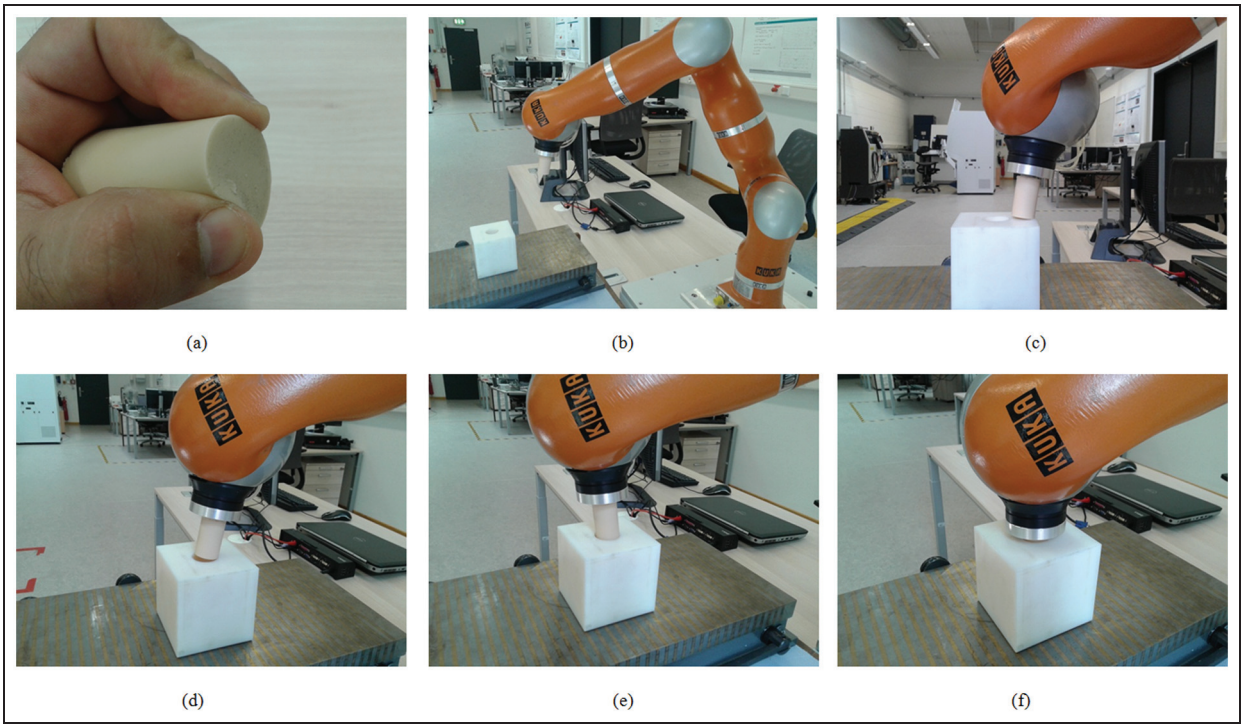

Figure 1. Test stand of experiment 1: (a) the flexible rubber object and its deformation when it is grasped, (b) Phase 1, (c) Phase 2, (d) Phase 3, (e) Phase 4, and (f) Phase 5.

$$\boldsymbol{f} = [f_x, f_y, f_z] \tag{1}$$

where f_x, f_y, and f_z are the forces along the x, y, and z axes, respectively. Consider that the vector of the torque signals of the object is

$$\boldsymbol{\tau} = [\tau_x, \tau_y, \tau_z] \triangleright \tag{2}$$

where τ_x, τ_y, and τ_z are the torques around the x, y, and z axes, respectively. Then, one can combine equation (1) and (2) to form the wrench signals $\boldsymbol{w}$ as

$$\boldsymbol{w} = [f_x, f_y, f_z, \tau_x, \tau_y, \tau_z] \tag{3}$$

Hence, each model has six input signals, say $\boldsymbol{x}_k = [x_{k,1}, x_{k,2}, \ldots, x_{k,6}]$ with k to be the sample index. The CS modelling problem can be formulated as

$$y_k = \begin{pmatrix} 1 & \text{if } (x_k \in \text{current CF}) \\ 0 & \text{Otherwise} \end{pmatrix} \tag{4}$$

where y_k is the output of the CS model. It is worth noting that equation (4) is a classification problem and it represents a nonlinear mapping between x_k and y_k. The goal of almost all modelling and classification researches is to approximate or realise this mapping as accurate as possible. The next section explains the methodology that will be used throughout this article in realising equation (4).

DSM-GMM

The DSM-GMM is based on the blending of the Bayesian modelling (or classification), Gaussian mixtures model (GMM), and distribution similarity measure (DSM). Hence, these concepts are explained before detailing the DSM-GMM.

Bayesian classification

In the Bayesian classification, one can say that a given data vector $\boldsymbol{x}_k = [x_{k,1}, x_{k,2}, \ldots, x_{k,D}]$ belongs to one of the classes $\{c_1, c_2, \ldots, c_C\}$ if that class posterior probability is greater than that of the other classes. D is the width of the given data vector (for the CS modelling problem addressed in this article, it is clear that $D = 6$ and each model has six inputs), $\{c_1, c_2, \ldots, c_C\}$ is the set of classes, and C is the total number of classes. More explicitly, the data vector x_k belongs to class c_i, $i \in \{1, 2, \ldots, C\}$ if[41]

$$p(c_i|\boldsymbol{x}_k) \geqslant p(c_j|\boldsymbol{x}_k) \tag{5}$$

for all $j \in \{1, 2, \ldots, C\}$ with $i \neq j$. $p(c_i|\boldsymbol{x}_k)$ and $p(c_j|\boldsymbol{x}_k)$ are called the posterior probabilities of classes c_i and c_j, respectively, given the vector $\boldsymbol{x}_k$. So, equation (5) means that $\boldsymbol{x}_k$ belongs to class c_i provided that its posterior probability is greater than the posterior probabilities of all other classes c_j. The posterior probability $p(c_i|\boldsymbol{x}_k)$ is computed using the Bayes rule as

$$p(c_i|x_k) = \frac{p(x_k|c_i)p(c_i)}{p(x_k)} \tag{6}$$

where $p(\boldsymbol{x}_k|c_i)$ is the probability density function (PDF) of class c_i in the vector space of $\boldsymbol{x}_k$, $p(c_i)$ is the priori probability which is simply the probability of class c_i,

and $p(\boldsymbol{x}_k)$ is the probability of the data vector $\boldsymbol{x}_k$. Using the basics of the probability theory, one can determine $p(\boldsymbol{x}_k)$ as

$$p(\boldsymbol{x}_k) = \sum_{i=1}^{C} p(\boldsymbol{x}_k|c_i)p(c_i) \tag{7}$$

where $p(c_j|\boldsymbol{x}_k)$ can be computed using equations (6) and (7) by replacing the index i with j. Substituting equations (6) and (7) into equation (5) results

$$\frac{p(\boldsymbol{x}_k|c_i)p(c_i)}{\sum_{i=1}^{C} p(\boldsymbol{x}_k|c_i)p(c_i)} \geqslant \frac{p(\boldsymbol{x}_k|c_j)p(c_j)}{\sum_{j=1}^{C} p(\boldsymbol{x}_k|c_j)p(c_j)} \tag{8}$$

One can see that the denominators of the left- and right-hand sides of equation (8) are equal. Therefore, equation (8) can be re-written as

$$p(\boldsymbol{x}_k|c_i)p(c_i) \geqslant p(\boldsymbol{x}_k|c_j)p(c_j) \tag{9}$$

For equal priori probabilities $p(c_i)$ for all $i \in \{1, 2, \ldots, C\}$, one can say from equation (9) that the best approximation of the term $p(\boldsymbol{x}_k|c_i)$ results in the best modelling and classification for the pattern $\boldsymbol{x}_k$. In the conventional Bayesian classifier, a Gaussian distribution is used in approximating the term $p(x_k|c_j)$, that is

$$p(\boldsymbol{x}_k|c_i) = \frac{1}{(2\pi)^{D/2}|\Sigma|^{\frac{1}{2}}} exp\left(-\frac{1}{2}(\boldsymbol{x}_k - \boldsymbol{\mu})^T \sum^{-1}(x_k - \mu)\right) \tag{10}$$

where $\boldsymbol{\mu} \in R^D$ is the mean, $\boldsymbol{\Sigma} \in R^{D \times D}$ is the covariance matrix, and $|\boldsymbol{\Sigma}|$ is the determinant of $\boldsymbol{\Sigma}$. It was shown that the approximation of equation (10) performs well in the cases of normal distribution. However, in many situations, one may face cases in which the vector space signals, or several signals of the vector space, have non-normal distribution, and consequently, the use of equation (10) would result in increased modelling errors.

GMM

In order to accommodate the possible non-normal distribution of the signals, Gaussian mixtures are employed in modelling the features (input signals), that is, assigning more than a Gaussian component for each feature. Suppose that a single Gaussian distribution is represented as

$$N(\boldsymbol{x}_k, \boldsymbol{\mu}, \boldsymbol{\Sigma}) = \frac{1}{|2\pi|^{D/2}|\boldsymbol{\Sigma}|^{\frac{1}{2}}} exp\left(-\frac{1}{2}(\boldsymbol{x}_k - \mu)^T \sum^{-1}(\boldsymbol{x}_k - \boldsymbol{\mu})\right) \tag{11}$$

One can describe a GMM as

$$p(\boldsymbol{x}_k|c_i) = \sum_{q=1}^{M} \omega_q N_q\left(\boldsymbol{x}_k, \mu_q, \boldsymbol{\Sigma}_q\right) \tag{12}$$

where M is the total number of the Gaussian mixtures; ω_q, $\boldsymbol{\mu}_q$, and $\boldsymbol{\Sigma}_q$ are the weight, mean, and covariance of the qth Gaussian component, respectively. Suppose that $\boldsymbol{\omega} = [\omega_1, \omega_2, \ldots, \omega_M]$, $\boldsymbol{\mu} = [\boldsymbol{\mu}_1, \boldsymbol{\mu}_2, \ldots, \boldsymbol{\mu}_M]$, $\boldsymbol{\Sigma} = [\boldsymbol{\Sigma}_1, \boldsymbol{\Sigma}_2, \ldots, \boldsymbol{\Sigma}_M]$, and $\theta = (\omega_1, \boldsymbol{\mu}_1, \boldsymbol{\Sigma}_2, \ldots, \omega_M, \boldsymbol{\mu}_M, \boldsymbol{\Sigma}_M)$. The model of equation (12) can be written in terms of the parameters θ as

$$p(\boldsymbol{x}_k|c_i; \boldsymbol{\theta}) = \sum_{q=1}^{M} \omega_q N_q\left(\boldsymbol{x}_k, \boldsymbol{\mu}_q, \boldsymbol{\Sigma}_q\right) \tag{13}$$

Finding the best parameter set $\boldsymbol{\theta}$, that optimises the models from the available measurements, would enhance the performance of the classification process.

EM

One of the most efficient approaches in finding the parameter set $\boldsymbol{\theta}$ is the EM algorithm. The EM algorithm is composed of two steps: the E-step in which the log-likelihood is estimated for the current parameters, and the M-step in which the parameter $\boldsymbol{\theta}$ is updated such that a maximised log-likelihood would result. In order to explain the EM algorithm, let us consider the overall data $\mathbf{X} = [\boldsymbol{x}_1, \boldsymbol{x}_2, \ldots, \boldsymbol{x}_N]^T$. Then, the likelihood function for the data $\mathbf{X}$ given the parameter set θ can be defined as

$$\ell(\mathbf{X}; \boldsymbol{\theta}) = \prod_{n=1}^{N} p(\boldsymbol{x}_n; \boldsymbol{\theta}) \tag{14}$$

Define the logarithm of $\ell(\boldsymbol{X}; \boldsymbol{\theta})$ to be $L(\boldsymbol{X}; \boldsymbol{\theta})$ which is called the log-likelihood. Taking the logarithm for both sides of equation (14), then the log-likelihood can be expressed as

$$L(\boldsymbol{X}; \boldsymbol{\theta}) = \sum_{n=1}^{N} \ln(p(\boldsymbol{x}_n; \boldsymbol{\theta})) \tag{15}$$

The parameter set $\boldsymbol{\theta}$ that maximises equation (15) can be described as

$$\boldsymbol{\theta}(t) = \arg\max_{\theta} L(\mathbf{X}; \boldsymbol{\theta}(\boldsymbol{\tau})) \tag{16}$$

subject to

$$\sum_{q=1}^{M} \omega_q = 1$$

where equation (16) is a constrained optimisation problem and the analytical solutions can be intractable. Therefore, iterative solutions, like the EM algorithm, were suggested to solve such a problem. An important quantity that plays a vital role in the EM algorithm is the conditional probability of y given $\mathbf{X}$ and let us denote $p(c_i = 1|\boldsymbol{x}_k)$ as $\gamma(c_{ik})$. The value of $\gamma(c_{ik})$ can be computed using the Bayes rule as

$$\gamma(c_{ik}) = \frac{p(c_i = 1)p(\boldsymbol{x}_k|c_i = 1)}{\sum_{q=1}^{M} p(c_q = 1)p(\boldsymbol{x}_k|z_q = 1)} \quad (17)$$

that leads to

$$\gamma(c_{ik}) = \frac{w_i N_i(\boldsymbol{x}_k, \boldsymbol{\mu}_i, \boldsymbol{\Sigma}_i)}{\sum_{q=1}^{M} w_q N_q\left(\boldsymbol{x}_k, \boldsymbol{\mu}_q, \boldsymbol{\Sigma}_q\right)} \quad (18)$$

$\gamma(c_{ik})$ is called the responsibility that the ith component takes for explaining $\boldsymbol{x}_k$.[41] The following steps summarise the EM algorithm:

Step 1. Initialise the parameter set $\boldsymbol{\theta} = (\omega_1, \boldsymbol{\mu}_1, \boldsymbol{\Sigma}_2, \ldots, \omega_M, \boldsymbol{\mu}_M, \boldsymbol{\Sigma}_M)$. Initialise the convergence parameters ε and ε;
Step 2. (E-Step) For the current parameter set $\boldsymbol{\theta}$ compute the responsibilities using equation (18);
Step 3. (M-Step) Re-estimate the parameters using the current responsibilities

$$\boldsymbol{\mu}_i^{new} = \frac{1}{N_i}\sum_{n=1}^{N} \gamma(c_{in})\boldsymbol{x}_n \quad (19)$$

$$\sum_i^{new} = \frac{1}{N_i}\sum_{n=1}^{N} \gamma(c_{in})\left(\boldsymbol{x}_n - \boldsymbol{\mu}_i^{new}\right)\left(\boldsymbol{x}_n - \boldsymbol{\mu}_i^{new}\right)^T \quad (20)$$

$$\omega_i^{new} = \frac{N_i}{N} \quad (21)$$

with

$$N_i = \sum_{n=1}^{N} \gamma(c_{in}) \quad (22)$$

Step 4. Compute the log-likelihood

$$\ln p(\mathbf{X}; \boldsymbol{\theta}) = \sum_{n=1}^{N} \ln\left\{\sum_{i=1}^{M} \omega_i N(\boldsymbol{x}_n, \boldsymbol{\theta})\right\} \quad (23)$$

Step 5. Check for the convergence
If $|\boldsymbol{\theta}^{new} - \boldsymbol{\theta}| \leqslant \varepsilon$ or $|\ln p(\mathbf{X}; \boldsymbol{\theta}^{new}) - \ln p(\mathbf{X}; \boldsymbol{\theta})| \leqslant \varepsilon$ then stop. Otherwise, go to Step 2.

See the book authored by Bishop[42] or other related monograph for more details on the EM algorithm and the derivations of the equations above. Even though the EM algorithm results in desirable GMM parameters, the choice of the number of GMM components remains important in having an optimal modelling of the given data. In the next subsection, a simple and reasonable approach is proposed for the identification of the optimal number of GMM components. Incorporating the identification process of the number of GMM components in the proposed CS modelling scheme would significantly enhance the modelling of the captured signals.

DSM

One of the crucial elements that quantifies the efficiency of data-driven models is the similarity between the developed models and the distribution of the given signals. For instance, let's consider the histogram shown in Figure 2(a), which is taken for the torque signal around the x-axis of one of the experiments. In order to see the optimal number of GMM components that can optimally model this signal, it is needed to find the number of GMM components that gives the highest similarity between the developed model and the signal distribution. Different approaches were developed in quantifying the similarity between two distributions;

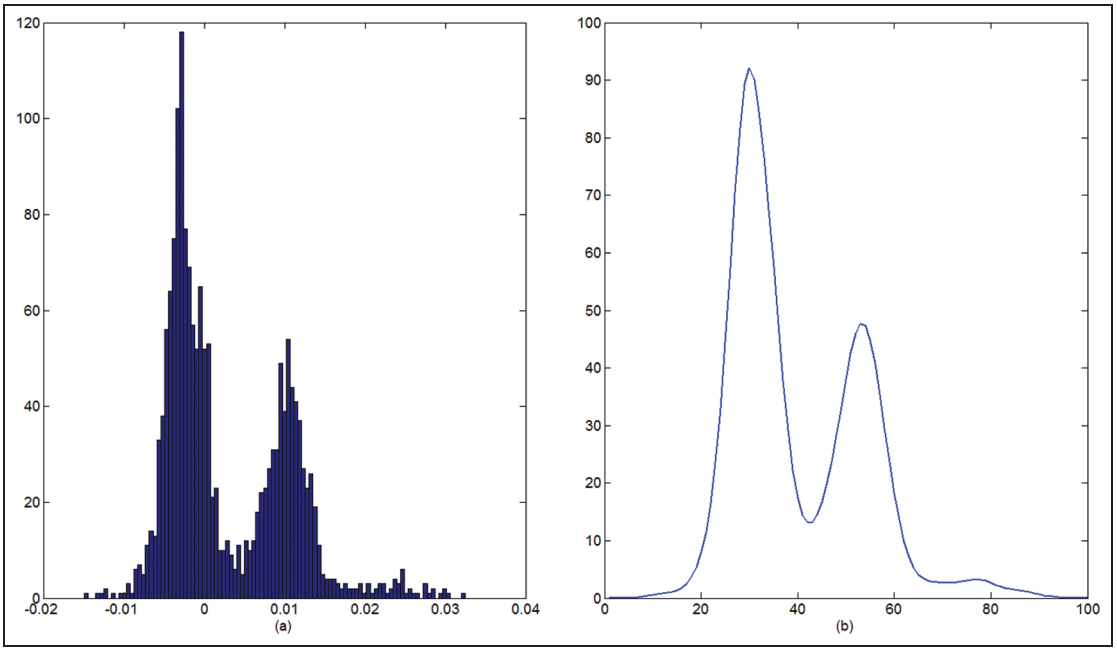

Figure 2. (a) τ_x histogram and (b) τ_x optimal GMM model.

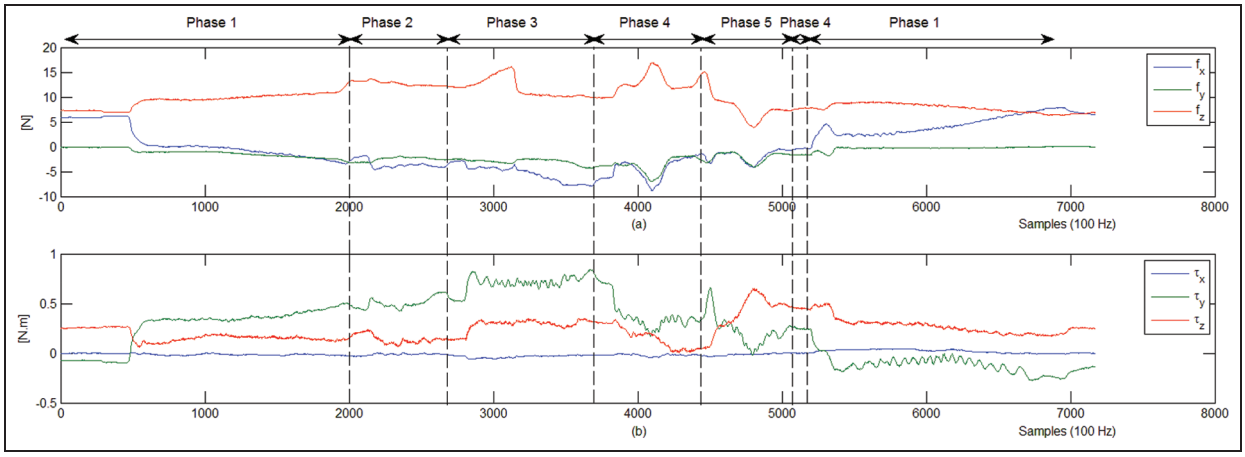

Figure 3. Experiment 1: training signals: (a) force signals [N] and (b) torque signals [N m].

however, probabilistic similarity measure (PSM) is considered as one of the most effective similarity measure schemes. In the PSM, the CSR performance is used as an index for the similarity measure between the histogram of Figure 2(a) and the developed model.[42] The best CSR results from the highest similarity between the developed models and the signals histograms. For the example of Figure 2(a), the best CSR results with three GMM components. Figure 2(b) shows the GMM that can optimally model the given histogram. If we increase or decrease the number of GMM components, then the similarity between the histogram of the signal and the developed model is decreased causing CSR degradation.

In the framework of DSM, the number of GMM that optimally models the CS from the given wrench signals can be estimated and enhanced CS modelling scheme would be resulted. The next section explains the experimental validation when using the DSM-GMM for modelling the CS of robotic peg-in-hole assembly process with flexible rubber materials.

Experimental validation

For evaluating the performance of the proposed DSM-GMM CS modelling scheme, a test stand was built that is composed of a KUKA LWR doing peg-in-hole assembly tasks of flexible rubber materials. The key features of the KUKA LWR are detailed in LWR 4+ specification.[43] The KUKA LWR is equipped with appropriate sensors that enable researchers in capturing the wrench signals of the manipulated object through an fast research interface (FRI) port which is installed within the robot hardware. The FRI port is connected to a remote PC that performs the computational aspects of the modelling process. The features of the PC used in the experiments are Intel® Core™ i5-2540 CPU with 2.6 GHz speed and 4 GB RAM running under a Linux environment. The rate of communication between the remote PC and the robot, through the FRI, is 100 Hz. The programming is done in a C++ platform. In order to see the performance of the suggested DSM-GMM CS modelling scheme, two experiments are conducted for two flexible rubber objects with different stiffness values. For both experiments, the tolerances, say ε and ε, are chosen to be 1×10^{-9}.

Experiment 1

In this experiment, the assembly of a flexible rubber manipulated object (peg) is considered in evaluating the performance of the proposed DSM-GMM CS modelling scheme. The object is made from Neukasil RTV 230 which is a plastic silicone rubber material with hardness of 30 Shore A (see Appendix 1 for more features of this rubber material). Figure 1(a) shows the considered flexible rubber peg that can be deformed when grasped. Figure 1(b)–(f) shows different phases of the peg-in-hole assembly process. When executing the task of Figure 1, the wrench signals of the peg were captured and plotted as shown in Figure 3. The captured wrench signals were segmented into their corresponding phases and they were considered as training data. Using the DSM-GMM scheme, along with the training signals, a model is developed for each phase. Three Gaussian components were considered for each model and the justification for using this number of components will be detailed shortly afterwards.

In order to test the performance of the developed models, the same peg-in-hole assembly process was repeated again with re-capturing the wrench signals that are considered as test signals. Figure 4 shows the wrench test signals used for evaluating the performance of the DSM-GMM CS modelling scheme. There are five models and the one resulting with the highest likelihood is assigned with 1 for the output and all the rest are assigned with 0 outputs. As per using the CS models, that were developed by the DSM-GMM CS modelling scheme, in classifying the test signals shown in Figure 4, the models outputs were evaluated and plotted in Figure 5. For the test set of Figure 4, it has 7175 samples and when using the DSM-GMM CS

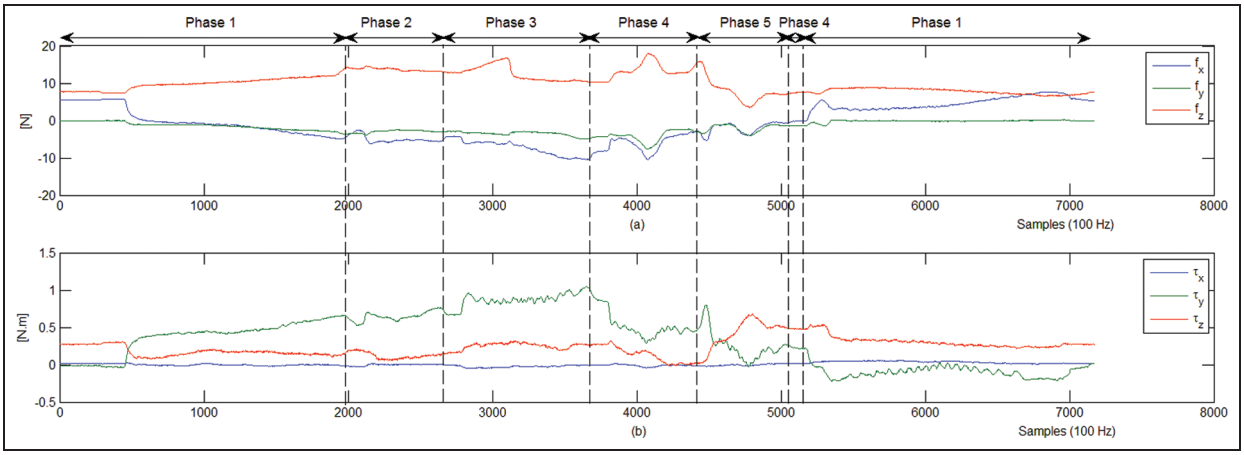

Figure 4. Experiment 1: test signals: (a) force signals [N] and (b) torque signals [N m].

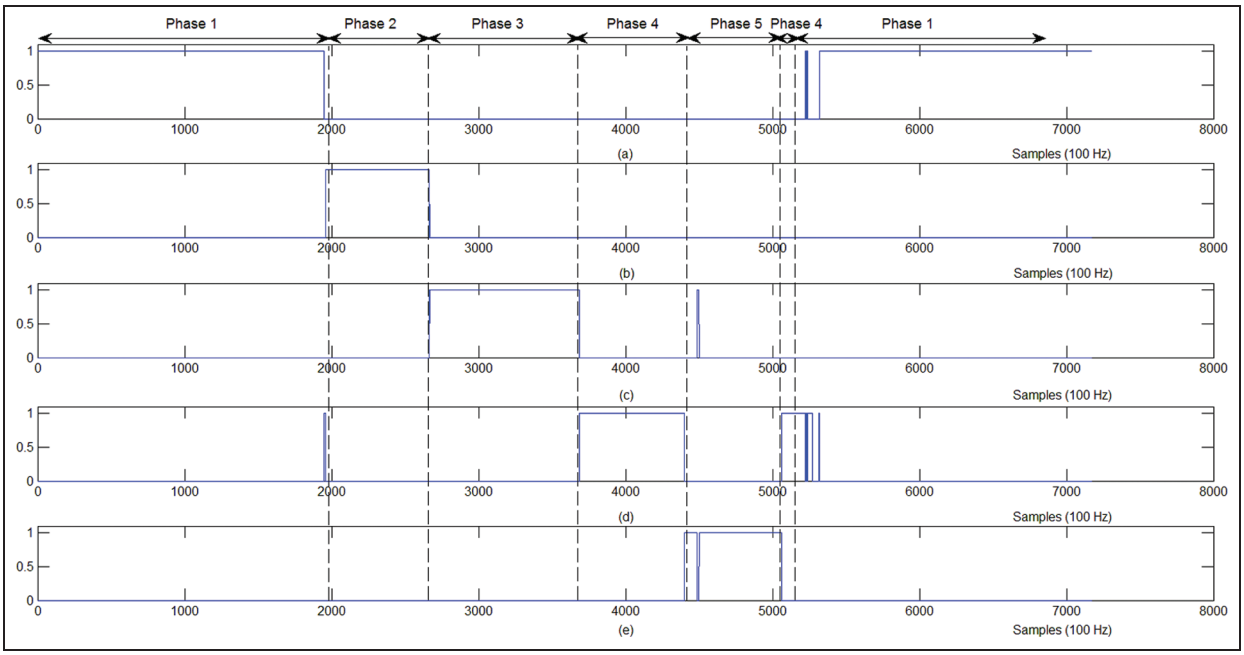

Figure 5. Experiment 1: DSM-GMM CS models outputs: (a) Phase 1, (b) Phase 2, (c) Phase 3, (d) Phase 4, and (e) Phase 5.

modelling scheme, 6774 samples were correctly classified and the rest were misclassified. As a result, the CSR for the DSM-GMM is computed to be 94.4%. For the sake of comparison, we developed the corresponding models using the SVM-FIM,[36] the GS-FCA,[38] the SGB,[34] and the CFC.[20] The total number of correctly classified samples were found to be 4729, 4606, 4356, and 1959 samples for the GS-FCA, SVM-FIM, SGB, and CFC schemes, respectively. One can compute the CSR to be 65.9%, 64.2%, 60.7%, and 27.3% for the GS-FCA, SVM-FIM, SGB, and CFC modelling schemes, respectively. Comparing the performance of the DSM-GMM with the rest, we can see that the DSM-GMM CS modelling scheme is outperforming the rest. The main two reasons behind such superiority of the DSM-GMM scheme are the accommodation of the non-stationary behaviour of the signals through the use of the GMM in building the likelihood functions and using the EM in computing the GMM components such that the log-likelihood is maximised. In order to see the non-stationary nature of the captured signals, the samples of Phase 3 were taken as an example and the histograms of the training signals, of this phase, were sketched. Figure 6 shows the histograms of Phase 3 signals. One can see that almost all signals are having non-normal distribution, that is, non-stationary behaviour. Therefore, the use of the DSM-GMM results in optimal likelihoods for the underlying signals that would significantly enhance the performance of the suggested CS modelling approach. The computational time (CT), that is, the time required for developing the models, of the DSM-GMM, GS-FCA, SVM-FIM, SGB, and CFC modelling schemes was measured and found to be 18.795, 237.307, 70.719, 92.083, and 0.002 s, respectively. Table 1 summarises the CSR and CT for all approaches mentioned above.

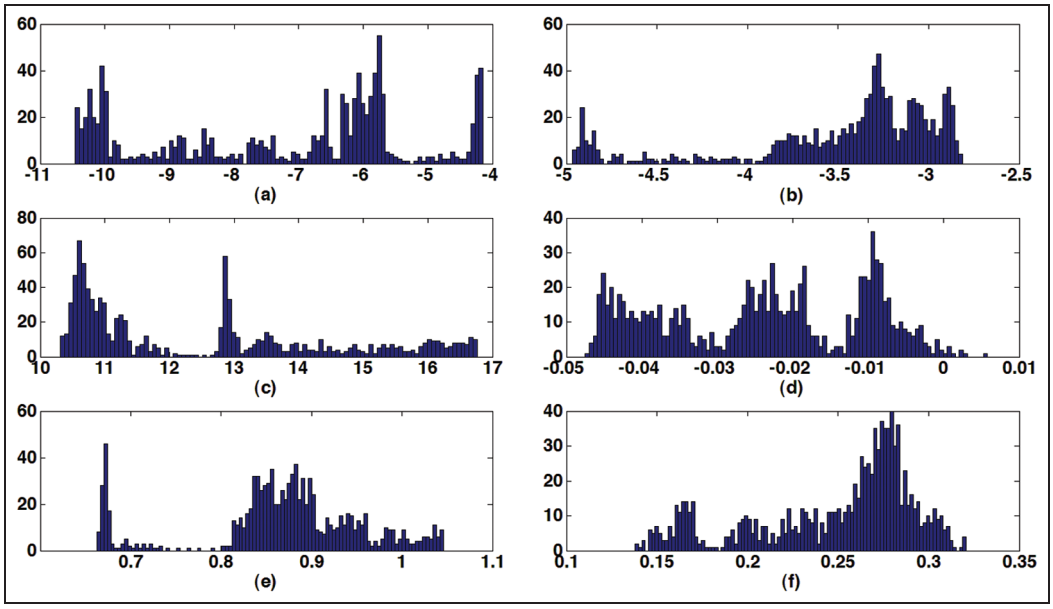

Figure 6. Experiment 1: signals histogram of Phase 3: (a) f_x, (b) f_y, (c) f_z, (d) τ_x, (e) τ_y, and (f) τ_z.

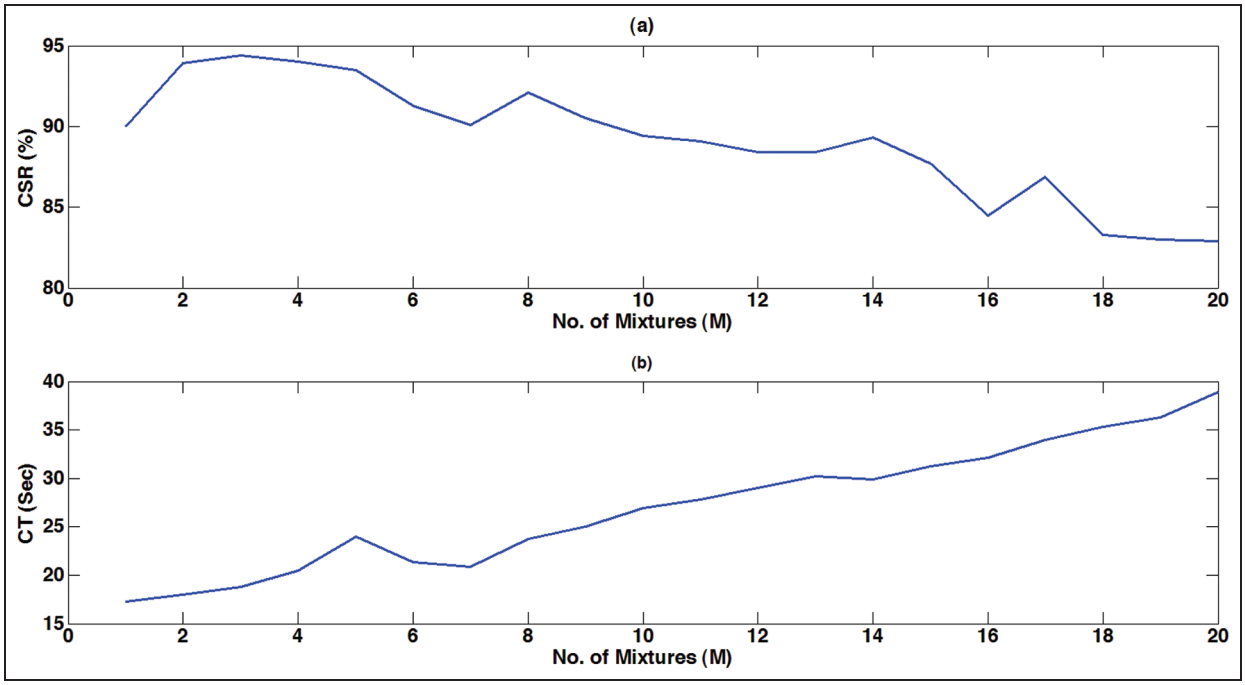

Figure 7. Experiment 1: DSM-GMM CS modelling scheme CSR and CT for different Gaussian components: (a) the CSR versus the number of Gaussian components (M) and (b) the CT versus the number of Gaussian components (M).

From Table 1, it can be seen that the DSM-GMM CS modelling scheme provides an excellent performance with a reduced CT. In order to see the effect of the number of Gaussian components, say M, on the CSR and CT of the DSM-GMM, the modelling process above was repeated for $M = 1, 2, 3..., 20$. For each value of M, the value of the CSR and CT were computed. Figure 7(a) and (b) shows the CSR and CT, respectively, versus the number of Gaussian components M. From Figure 7(a), it can be noticed that the highest CSR is 94.4% and such CSR was obtained for $M = 3$. Hence, one can have a strong impression with $M = 3$, the similarity between the developed models and the PDFs of the test signals is maximal. Indeed, such an approach of measuring the similarity between different PDFs is called probabilistic histogram similarity measure and the CSR is considered an index for judging the PDF's similarity.[42] From

Figure 7(b), it is obvious that the CT is not minimal for $M = 3$. However, the highest CSR of 94.4% with CT of 18.795 s, considering three Gaussian components for each CS model are appealing.

Experiment 2

This experiment considers a less stiff manipulated object for the given peg-in-hole assembly task. The utilised material is Neukasil RTV 23 which is a plastic silicone rubber with hardness of 6 Shore A (see Appendix 2 for more features of this material). Figure 8 shows the peg-in-hole assembly process of experiment 2 which is similar to that of experiment 1 except for the manipulated object. When executing the peg-in-hole assembly process of Figure 8, the wrench signals were captured for different phases of the given task. Figure 9 shows the captured wrench signals and using the DSM-GMM CS modelling scheme, a model was developed for each phase. Four Gaussian components were used for each model. In order to evaluate the performance of the developed models, the task of Figure 8 was repeated again and the corresponding wrench signals were re-captured, as shown in Figure 10, that are considered as test signals. Using the signals of Figure 10 as inputs to the developed DSM-GMM CS models, we obtained the model outputs shown in Figure 11. The total number of the test samples is 6749 and using the DSM-GMM CS modelling scheme, 6351 samples were correctly classified. When using the available CS modelling schemes, the number of correctly classified samples was found to be 4218, 4097, 3921, 3806, and 1762 samples for the GS-FCA, SVM-FIM, SGB, and CFC modelling schemes. One can compute the CSR for the DSM-GMM, GS-FCA, SVM-FIM, SGB, SVM-FIM, and CFC modelling schemes to be 94.1%, 62.5%, 58.1%, 56.4%, and 26.1%, respectively. Furthermore, the CT was measured to be 20.491, 221.931, 66.317, 85.816, and 0.002 s for the DSM-GMM, GS-FCA, SVM-FIM, SGB, and CFC schemes, respectively. Therefore, one can say that the DSM-GMM CS modelling scheme provides an excellent CSR performance with a reduced CT. Table 2 summarises the CSR and CT for all CS modelling schemes considered in this experiment.

Table 1. Experiment 1: CSR and CT for the DSM-GMM, GS-FCA, SVM-FIM, SGB, and CFC CS modelling approaches.

Approach	CSR (%)	CT (s)
DSM-GMM	94.4	18.795
GS-FCA	65.9	237.307
SVM-FIM	64.2	70.719
SGB	60.7	92.083
CFC	27.3	0.002

CFC: conventional fuzzy classifier; CSR: classification success rate; CT: computational time; DSM-GMM: distribution similarity measure–based Gaussian mixtures mode; GS-FCA: gravitational search-fuzzy clustering algorithm; SGB: stochastic gradient boosting; SVM-FIM: support vector machine–based fuzzy inference mechanism.

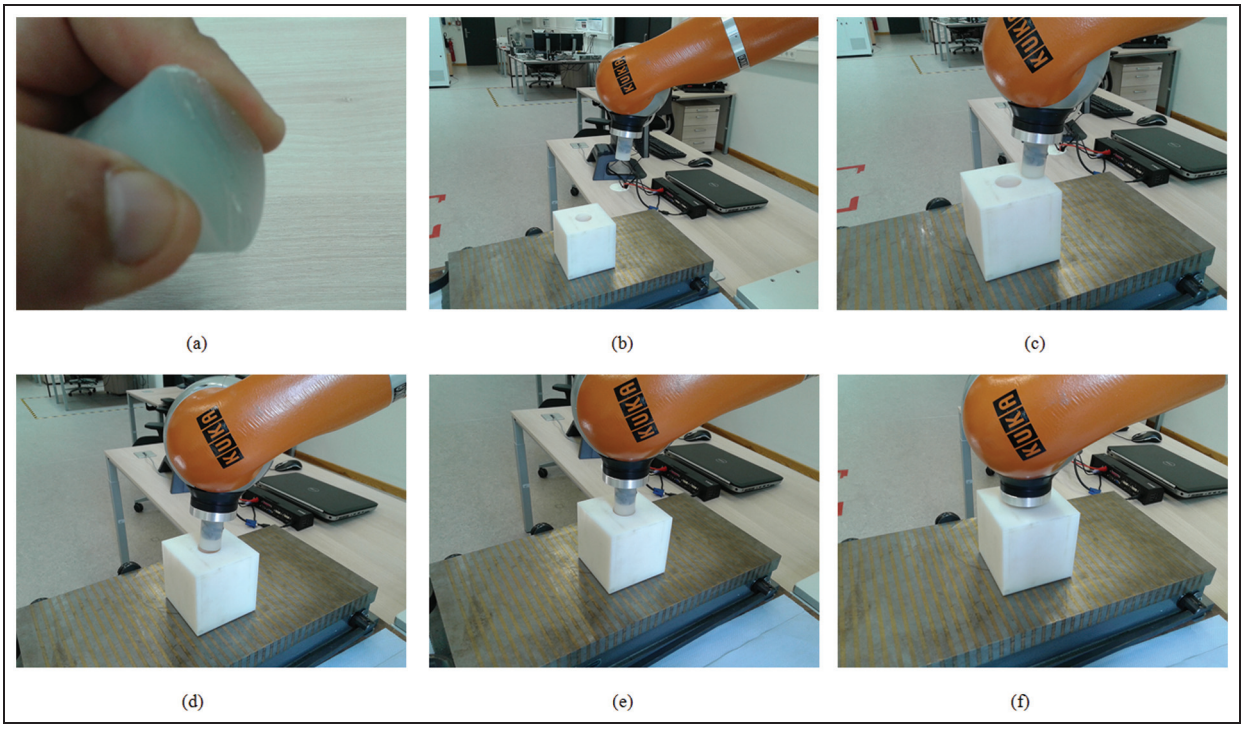

Figure 8. Test stand of experiment 2: (a) the flexible rubber object and its deformation when it is grasped, (b) Phase 1, (c) Phase 2, (d) Phase 3, (e) Phase 4, and (f) Phase 5.

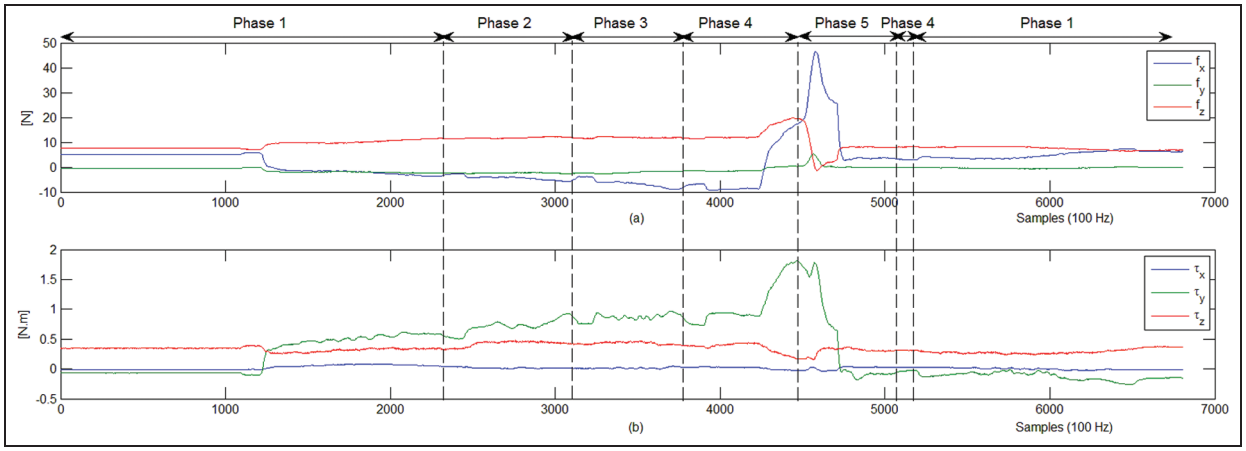

Figure 9. Experiment 2: training signals: (a) force signals [N] and (b) torque signals [N m].

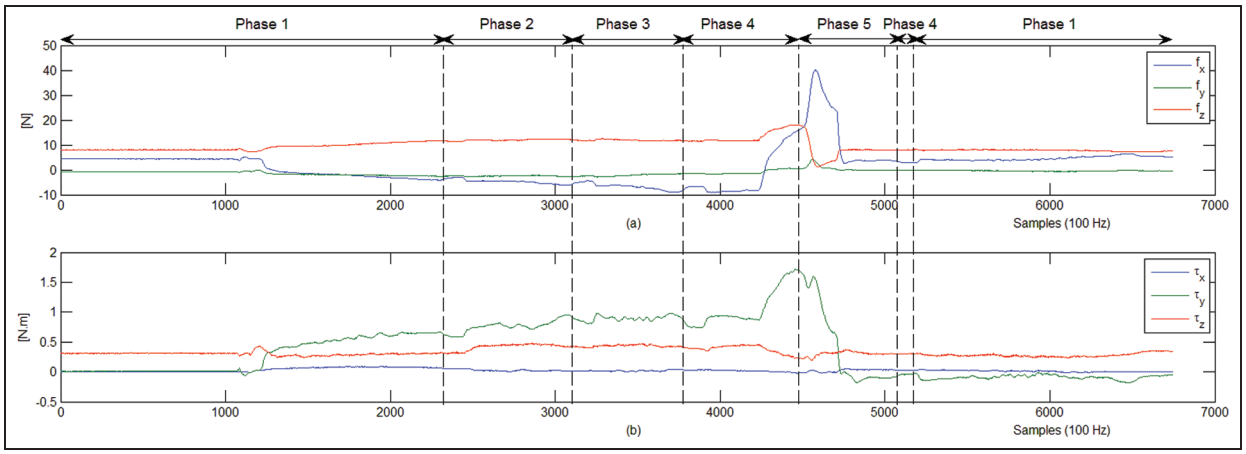

Figure 10. Experiment 2: test signals: (a) force signals [N] and (b) torque signals [N m].

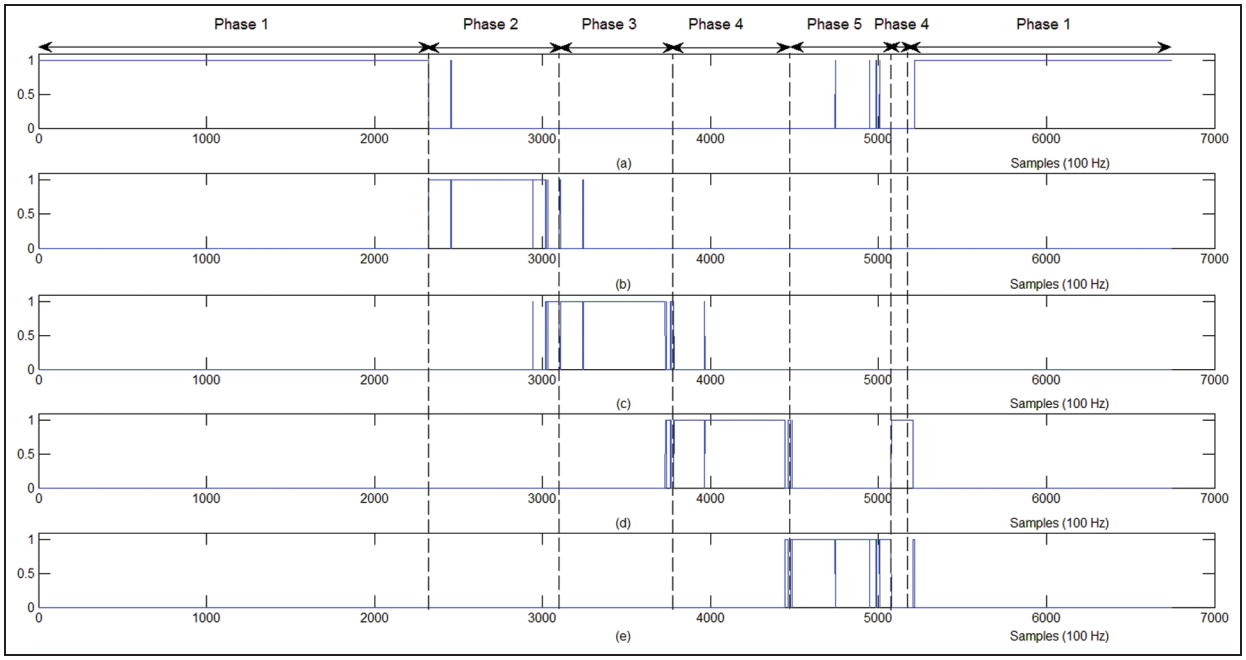

Figure 11. Experiment 2: DSM-GMM CS models outputs: (a) Phase 1, (b) Phase 2, (c) Phase 3, (d) Phase 4, and (e) Phase 5.

The superiority of the DSM-GMM CS modelling scheme stems from the accommodation of the signals non-stationarity, by employing the GMM, in modelling the signals and the use of the EM algorithm in finding the parameters of the GMM likelihoods for each signal. In order to see the non-stationary behaviour of the signals, Phase 4 is taken as an example and plotted the histograms of its signals and as shown in Figure 12. It is clear that all signals are non-stationary. The signals of other phases are also non-stationary and their histograms were not graphed for saving space. Hence, an excellent PDF's similarity, between the developed models and the captured signals, is achieved that results in enhanced CSR performance. The experiment above was repeated for different numbers of Gaussian components, say $M = 1, 2, 3, \ldots, 20$, with computing the CSR and measuring the CT for each value of M. Figure 13 shows the CSR and CT versus the number of Gaussian components, say M, and it is clear that the best CSR is obtained with $M = 4$. Hence, one can deduce that the highest similarity, between the distribution of the developed models and that of the captured signals, is obtained for $M = 4$ that gives a good reason to choose this number of components for each CS model. For the CT, one can roughly say that it increases as the number of components increases.

Table 2. Experiment 2: CSR and CT for The DSM-GMM, GS-FCA, SVM-FIM, SGB, and CFC CS modelling approaches.

Approach	CSR (%)	CT (s)
DSM-GMM	94.1	20.491
GS-FCA	62.5	221.931
SVM-FIM	60.7	66.317
SGB	58.1	85.816
CFC	26.1	0.002

CFC: conventional fuzzy classifier; CSR: classification success rate; CT: computational time; DSM-GMM: distribution similarity measure–based Gaussian mixtures model; GS-FCA: gravitational search-fuzzy clustering algorithm; SGB: stochastic gradient boosting; SVM-FIM: support vector machine–based fuzzy inference mechanism.

Discussion

In order to have a clear vision of the justifications behind the superiority of the proposed DSM-GMM compared with the available CS modelling schemes, the following points were noted:

1. In addition to its sensitivity to the position variation, the EM-GMM CS modelling strategy reported by Jasim and Plapper[39] is not featuring optimised number of GMM components. In the direct application of the EM-GMM CS modelling scheme in experiment 2, with three GMM components, 6269 samples were correctly classified that gives a CSR of 92.9%. Compared to the 94.1% CSR obtained with the DSM-GMM, one can have a strong impression that due to optimising the number of the GMM components, optimal similarity, between the distribution of the captured signals and the developed models, was obtained. Hence, the non-optimised EM-GMM CS modelling reported by Jasim and Plapper[39] would not result in enhanced modelling performance as that obtained with the DSM-GMM. Stemming from this fact, one can deduce that including the optimisation of the number of the GMM components may even lead to further enhancements, specifically in the computational cost. Moreover, further enhancements can be brought about using minimal number of features for each CS model. Possible

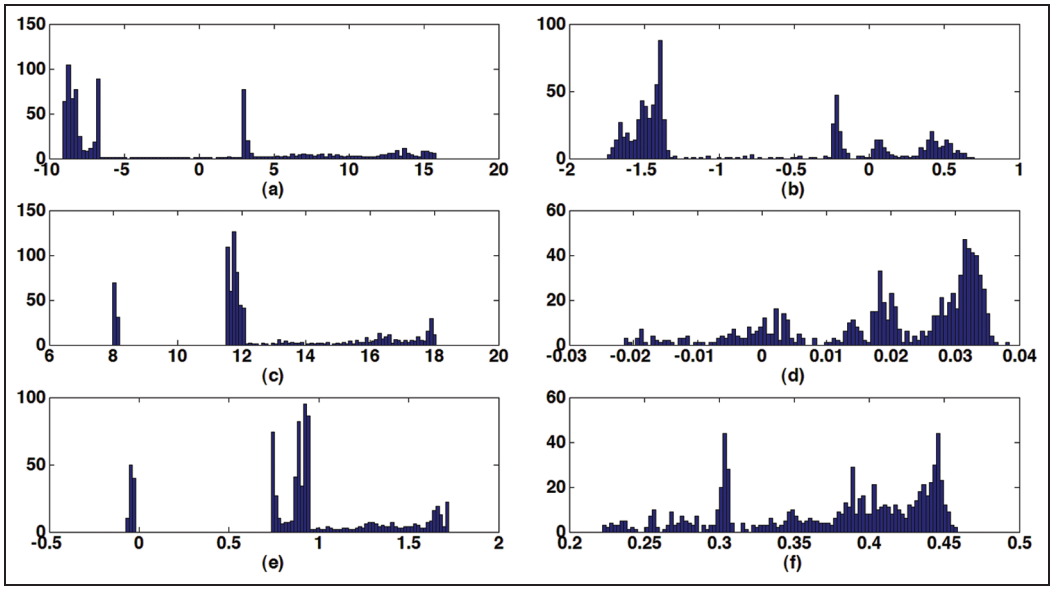

Figure 12. Experiment 2: signals histogram of Phase 4: (a) f_x, (b) f_y, (c) f_z, (d) τ_x, (e) τ_y, and (f) τ_z.

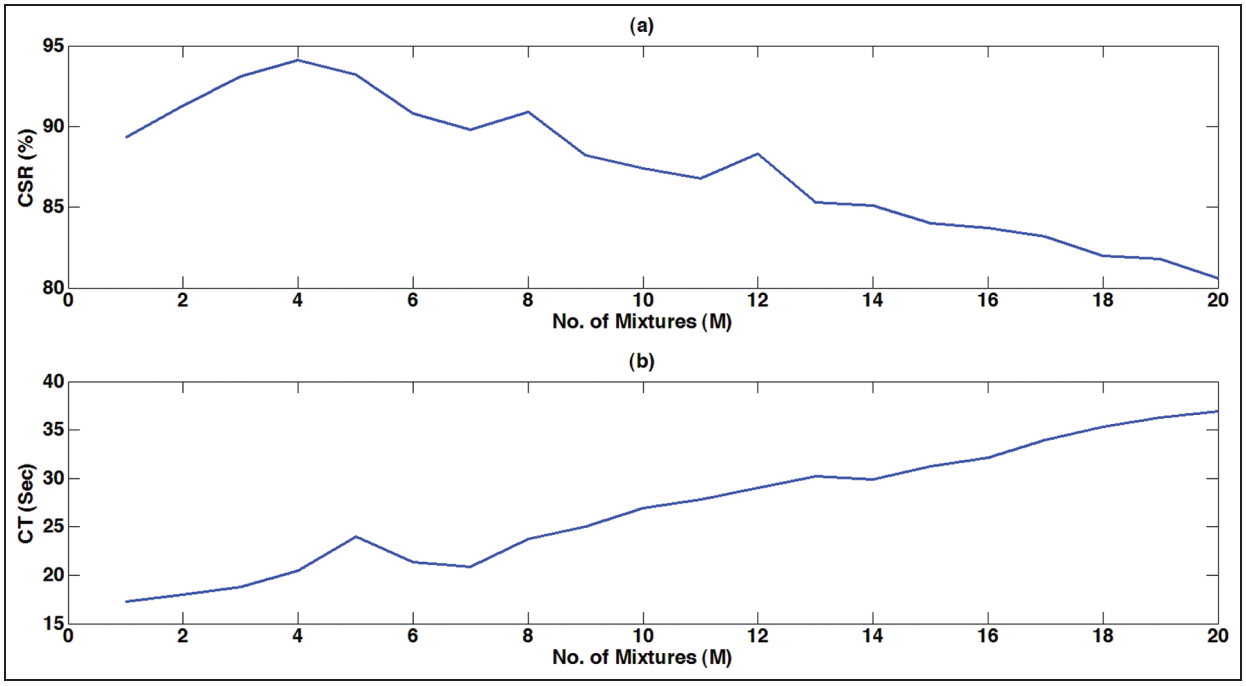

Figure 13. Experiment 2: DSM-GMM CS modelling scheme CSR and CT for different Gaussian components: (a) the CSR versus the number of Gaussian components (*M*) and (b) the CT versus the number of Gaussian components (*M*).

use of simultaneous optimisation of the number of GMM components and feature selection reported by Figueiredo and Jain,[44] Law et al.,[45] and Markley and Miller[46] or other relevant works might be suitable for the given situation. However, this requires further investigations, that is, left for future efforts.

2. Even though excellent CSR was reported by Jasim and Plapper[38] for the cube-in-corner assembly process of a rigid object, it can be seen from experiment 1 and experiment 2 that the CSR of the GS-FCA is suffering from a significant modelling inaccuracy for the case of peg-in-hole assembly of flexible objects. The use of fixed number of clusters (which is 7) for each CS model along with the fixed amplitude of 1 for each of the fuzzy set in the GS-FCA modelling scheme results in a significant dissimilarity between the distribution of the captured signals and the developed GS-FCA models, that is, directly influencing the CSR of the whole GS-FCA modelling performance. Likewise to the SVM-FIM CS classification scheme reported in Jakovljevic et al.,[36] even though efficient use of SVM assists in having efficient fuzzy sets, the fuzzy membership functions are indeed not reflecting precise distribution of the captured signals since fixed amplitude of 1 is used for the SVM-FIM as well. Whereas for the DSM-GMM CS modelling scheme, in addition to the optimised number of GMM components, the weights of the GMM play a vital role in having more accurate fit for the distribution of the captured signals bringing about a significant enhancement in the performance of the DSM-GMM.
3. The SGB strategy reported by Cabras et al.[34] is based on fitting linear models to the given training set such that

$$\Phi(F) = \sum_{k=1}^{N} L(y_k, F(\boldsymbol{x}_k)) \tag{24}$$

is minimised. $F(\boldsymbol{x}_k)$ is a linear fit of the model and $L(y_k, F(\boldsymbol{x}_k))$ is the loss function that quantifies for the misclassification of the pattern $\boldsymbol{x}_k$. As per using the deviance of the Bernoulli, $L(y_k, F(\boldsymbol{x}_k))$ was described to be

$$L(\boldsymbol{y}, \boldsymbol{F}) = -2(\boldsymbol{y}F(X) - log[1 + exp(F(\boldsymbol{X}))]) \tag{25}$$

Even though the SGB was shown to be very efficient in fitting the same data, equations (24) and (25) make this scheme to be very sensitive to the prediction of data samples other than the training set that might result misclassifications even for samples with slight deviations of the original training samples. Hence, a significant performance degradation would be expected when using the SGB classifier for the CS modelling of flexible parts assembly since object elasticity shrinks the possibility of having very much similar training and test signals. Moreover, equations (24) and (25) constitute a non-convex optimisation problem that could be trapped into local minima.

4. For the CFC modelling scheme proposed by Skubic and Volz,[20] the output of the *i*th CS model is computed using the fuzzy *if-then* rule

$$\text{if } x_{1,k} \text{ is } A_{i,1} \text{ and } \ldots x_{6,k} \text{ is } A_{i,6} \text{ then } y = CF_i \quad (26)$$

$A_{i,j}$ is the antecedent membership function of the jth input signal for the ith CS model. The Gaussian membership function is used for the antecedent part of the *if-then* rule above with the statistical mean and standard deviation used as the parameters of the membership functions. Hence, the CT is 0.002 s since it merely involves computing the mean and standard deviation of the training signals. However, the degraded performance of the CFC modelling scheme, with the CSR to be 27.3%, is a major drawback that makes such a scheme avoidable. Compared to the GS-FCA, SVM-FIM and SGB approaches, the DSM-GMM CS modelling scheme is having the least CT along with the highest CSR. Therefore, one can say that the DSM-GMM is of an enhanced performance in both accuracy and computational cost.

5. Comparing Tables 1 and 2, the CSR of the DSM-GMM is decreased by 0.3% due to the decrement in object stiffness. Such object stiffness decrement results in the increment of the non-stationary behaviour of the captured signals that required the increment of the number of Gaussian components for each CS model from 3 (for the object of experiment 1) to 4 (for the object of experiment 2). Regarding the other CS modelling schemes, they were degraded by 3.4%, 3.5%, 2.6%, and 1.2% for the GS-FCA, SVM-FIM, SGB, and CFC, respectively. Therefore, one can say that the DSM-GMM CS modelling scheme is more robust against object deformation due to the accommodation of the increment in non-stationarity degree of the captured signals by slightly increasing (or decreasing) the number of Gaussian components. It is worth noting that the requirement to increase the number of the Gaussian components in experiment 2, compared to the experiment 1, gives us a strong impression of the increment in the signals non-stationarity as the object stiffness decreases.

Conclusion

In this article, DSM-GMM was proposed for the contact-state (CS) modelling of force-controlled robotic peg-in-hole assembly processes with flexible rubber parts. In order to accommodate the signals non-stationarity, the DSM-GMM CS modelling scheme employs the GMM in modelling the captured wrench signals. EM is utilised for computing the GMM parameters and the DSM is used for finding the optimal number of GMM components. The CSR is considered as the DSM and number of GMM components resulting with the best CSR is considered as the optimal GMM number for modelling the captured signals. Hence, the DSM-GMM results in more accurate modelling performance even with multiple objects of different elasticity. Experiments were conducted on a KUKA LWR doing peg-in-hole assembly tasks of flexible rubber parts. Two experiments are studied; in the first one, a peg made from Neukasil RTV 230 material, which is an elastic silicone rubber material of hardness 30 Shore A, is considered. Using the DSM-GMM, excellent CSR was obtained and the optimal number of GMM components was found to be 3. For the second experiment, a softer manipulated object made from Neukasil RTV 23, which has hardness of 6 Shore A, is studied and outstanding CSR was obtained. However, the number of optimal GMM components for the second experiment was found to be 4. For comparison purposes, the corresponding CS models were developed for both experiments using the available CS modelling schemes like the GS-FCA, the SVM-FIM, the SGB, and the CFC. From the comparison, the superiority of the DSM-GMM CS modelling scheme is shown with a reduced computational cost. Learning parsimonious GMM models in which both optimal number of GMM components and minimal features to be computed in the learning process would significantly enhance the modelling performance and computational efforts for the CS modelling of flexible objects. However, this is left to future research efforts.

Acknowledgements

The authors would like to thank the teams of KUKA Roboter GmbH in Houthalen, Belgium and KUKA Labs in Augsburg, Germany for their support on the technical issues of the KUKA LWR.

Declaration of conflicting interests

The author(s) declared no potential conflicts of interest with respect to the research, authorship, and/or publication of this article.

Funding

The author(s) disclosed receipt of the following financial support for the research, authorship, and/or publication of this article: This work was supported by the Fonds National de la Recherche (FNR) in Luxembourg under grant number AFR-2955286.

References

1. Biao Z, Jianjun W, Rossano G, et al. Vision-guided robotic assembly using uncalibrated vision. In: *Proceedings of the 2011 IEEE international conference on mechatronics and automation*, Beijing, China, 7–10 August 2011, pp.1384–1389. New York: IEEE.
2. Muelaner JE, Wang Z and Maropoulos PG. Concepts for and analysis of a high accuracy and high capacity (HAHC) aerospace robot. *Proc IMechE, Part B: J Engineering Manufacture* 2011; 225(8): 1393–1399.
3. Jayaram K and Joshi SS. Design and development of a vision-based micro-assembly system. *Proc IMechE, Part B: J Engineering Manufacture*. Epub ahead of print 8 January 2015. DOI: 10.1177/0954405414560779.

4. Whitney DE. Quasi-static assembly of compliantly supported rigid parts. *J Dyn Syst: T ASME* 1982; 104(1): 65–77.
5. Haskiya W, Maycock K and Knight JAG. A passive compliant wrist for chamferless peg-in-hole assembly operation from vertical and horizontal directions. *Proc IMechE, Part B: J Engineering Manufacture* 1998; 212(6): 473–478.
6. Desai RS and Volz RA. Identification and verification of termination conditions in fine motion in presence of sensor errors and geometric uncertainties. In: *Proceedings of the 1989 IEEE international conference on robotics and automation*, Scottsdale, AZ, 14–19 May 1989, pp.800–807. New York: IEEE.
7. Hirai S and Iwata K. Recognition of contact state based on geometric model. In: *Proceedings of the 1992 IEEE international conference on robotics and automation*, Nice, 12–14 May 1992, pp.1507–1512. New York: IEEE.
8. McCarragher BJ. Petri net modeling for robotic assembly and trajectory planning. *IEEE T Ind Electron* 1994; 41(6): 631–640.
9. Cao T and Sanderson AC. Task decomposition and analysis of robotic assembly task plans using Petri nets. *IEEE T Ind Electron* 1994; 41(6): 620–630.
10. Farahat AO, Graves BS and Trinkle JC. Identifying contact formations in the presence of uncertainty. In: *Proceedings of the 1995 IEEE/RSJ international conference on intelligent robots and systems*, Pittsburgh, PA, 5–9 August 1995, pp.59–64. New York: IEEE.
11. McCarragher BJ. Task primitives for the discrete event modeling and control of 6-DOF assembly tasks. *IEEE T Robotic Autom* 1996; 12(2): 280–289.
12. Chung SY and Lee DY. Discrete event systems approach to fixtureless peg-in-hole assembly. In: *Proceedings of the 2001 American control conference*, Arlington, VA, 25–27 June 2001, pp.4962–4967. New York: IEEE.
13. Hovland GE and McCarragher BJ. Combining force and position measurements for the monitoring of robotic assembly. In: *Proceedings of the 1997 IEEE/RSJ international conference on intelligent robots and systems*, Grenoble, 7–11 September 1997, pp.654–660. New York: IEEE.
14. Skubic M and Volz RA. Learning force sensory patterns and skills from human demonstration. In: *Proceedings of the 1997 IEEE international conference on robotics and automation*, Albuquerque, NM, 20–25 April 1997, pp.284–290. New York: IEEE.
15. Skubic M, Castrianni SP and Volz RA. Identifying contact formations from force signals: a comparison of fuzzy and neural network classifiers. In: *Proceedings of the 1997 international conference on neural networks*, Houston, TX, 9–12 June 1997, pp.1623–1628. New York: IEEE.
16. Iwata H and Sugano S. Human-robot-contact-state identification based on tactile recognition. *IEEE T Ind Electron* 2005; 52(6): 1468–1477.
17. Mosemann H, Raue A and Wahl F. Classification and recognition of contact states for force guided assembly. In: *Proceedings of the IEEE international conference on systems, man, and cybernetics*, San Diego, CA, 11–14 October 1998, pp.3400–3405. New York: IEEE.
18. Xiao J and Liu L. Contact states: representation and recognizability in the presence of uncertainties. In: *Proceedings of the 1998 IEEE/RSJ international conference on Intelligent Robots and Systems*, Victoria, BC, Canada, 13–17 October 1998, pp.1151–1156. New York: IEEE.
19. Everett LJ, Ravuri R, Volz RA, et al. Generalized recognition of single-ended contact formations. *IEEE T Robotic Autom* 1999; 15(5): 829–836.
20. Skubic M and Volz RA. Identifying single-ended contact formations from force sensor patterns. *IEEE T Robotic Autom* 2000; 16(5): 597–603.
21. Son C. A neural/fuzzy optimal process model for robotic part assembly. *Int J Mach Tool Manu* 2001; 41(12): 1783–1794.
22. Qiao H and Tso SK. Strategy investigation of precise robotic assembly operations with symmetric regular polyhedral objects. *Proc IMechE, Part B: J Engineering Manufacture* 1998; 212(7): 571–589.
23. Fei Y and Zhao X. An assembly process modeling and analysis for robotic multiple peg-in-hole. *J Intell Robotic Syst* 2003; 36: 175–189.
24. Cortesão R, Koeppem R, Nunes U, et al. Data fusion for robotic assembly tasks based on human skills. *IEEE T Robotic Autom* 2004; 20(6): 941–952.
25. Hovland GE and McCarragher BJ. Hidden Markov models as a process monitor in robotic assembly. *Int J Robot Res* 1998; 17(2): 153–168.
26. Lau HY. A hidden Markov model-based assembly contact recognition system. *Mechatronics* 2003; 13(8–9): 1001–1023.
27. Debus TJ, Dupot PE and Howe RD. Contact state estimation using multiple model estimation and Markov models. *Int J Robot Res* 2004; 23(4–5): 399–413.
28. Gadeyne K, Lefebvre T and Bruyninckx H. Bayesian hybrid model-state estimation applied to simultaneous contact formation recognition and geometrical parameter estimation. *Int J Robot Res* 2005; 24(8): 615–630.
29. Lefebvre T, Bruyninckx H and De Schutter J. Polyhedral contact formation identification for autonomous compliant motion: exact nonlinear Bayesian filtering. *IEEE T Robot* 2005; 21(1): 124–129.
30. Meeussen W, Rutgeerts J, Gadeyne K, et al. Contact-state segmentation using particle filters for programming by human demonstration in compliant motion tasks. *IEEE T Robot* 2007; 23(2): 218–231.
31. Thomas U, Molkenstruck S, Iser R, et al. Multi sensor fusion in robot assembly using particle filters. In: *Proceedings of the IEEE international conference on robotics and automation*, Rome, 10–14 April 2007, pp.3837–3843. New York: IEEE.
32. Katsura S, Matsumoto Y and Ohnishi K. Modeling of force sensing and validation of disturbance observer for force control. *IEEE T Ind Electron* 2007; 54(1): 530–538.
33. Okuda H, Takeuchi H, Inagaki S, et al. Modeling and analysis of peg-in-hole task based on mode segmentation. In: *Proceedings of the 2008 SICE annual conference*, Tokyo, Japan, 20–22 August 2008, pp.1595–1600. New York: IEEE.
34. Cabras S, Castellanos ME and Staffetti E. Contact-state classification in human demonstrated robot compliant motion tasks using the boosting algorithm. *IEEE T Syst Man Cy B* 2010; 40(5): 1372–1386.
35. Hertkorn K, Rao MA, Preusche C, et al. Identification of contact formations: resolving ambiguous force torque information. In: *Proceedings of the 2012 IEEE international conference on robotics and automation*, St. Paul, MN, 14–18 May 2012, pp.3278–3284. New York: IEEE.
36. Jakovljevic Z, Petrovic PB, Mikovic VD, et al. Fuzzy inference mechanism for recognition of contact states in

intelligent robotic assembly. *J Intell Manuf* 2014; 25(3): 571–587.
37. Abegg F, Remde A and Henrich D. Force-and vision-based detection of contact state transition. In: Henrich D and Wörm H (eds) *Robot manipulation of deformable objects*. London: Springer-Verlag, 2000, pp.112–134.
38. Jasim IF and Plapper PW. T-S fuzzy contact state recognition for compliant motion robotic tasks using gravitational search-based clustering algorithm. In: *Proceedings of the 2013 IEEE international conference on fuzzy systems*, Hyderabad, India, 7–10 July 2013, pp.1–8. New York: IEEE.
39. Jasim IF and Plapper PW. Contact-state monitoring of force-guided robotic assembly tasks using expectation maximization-based Gaussian mixtures models. *Int J Adv Manuf Tech* 2014; 73(5–8): 623–633.
40. Jasim IF, Plapper PW and Voos H. Position identification in force-guided robotic peg-in-hole assembly tasks. *Proc CIRP* 2014; 23: 217–222.
41. Bishop CM. *Pattern recognition and machine learning*. New York: Springer-Verlag, 2006.
42. Cha SH. Comprehensive survey on distance/similarity measures between probability density functions. *Int J Math Model Method Appl Sci* 2007; 1(4): 300–307.
43. *Lightweight robot 4 + specification* (Version: Spez LBR 4 + V5 en). KUKA Roboter GmbH, Augsburg, Germany 2011.
44. Figueiredo MAT and Jain AK. Unsupervised learning of finite mixture models. *IEEE T Pattern Anal* 2002; 24(3): 381–396.
45. Law MHC, Figueiredo MAT and Jain AK. Simultaneous feature selection and clustering using mixture models. *IEEE T Pattern Anal* 2004; 26(9): 1154–1166.
46. Markley SC and Miller DJ. Joint parsimonious modeling and model order selection for multivariate Gaussian mixtures. *IEEE J Sel Top Signa* 2010; 4(3): 548–559.

Appendix 1

Features of Neukasil RTV 230 rubber material

Viscosity = 9500 MPa s;
Hardness = 30 Shore A;
Tensile strength = 4.5 MPa;
Resistance to tear prorogation = 18 N/mm.

Appendix 2

Features of Neukasil RTV 23 rubber material

Viscosity = 3500 MPa s;
Hardness = 6 Shore A;
Tensile strength = 2 MPa;
Resistance to tear prorogation = 8 N/mm.